

## Feature Article

## Ultrathin Zn and ZnO films on Cu(111) as model catalysts



Bo-Hong Liu, Irene M.N. Groot, Qiushi Pan, Shamil Shaikhutdinov\*, Hans-Joachim Freund

Department of Chemical Physics, Fritz Haber Institute, Faradayweg 4-6, 14195, Berlin, Germany

## ARTICLE INFO

## Keywords:

Thin oxide films  
Surface structures  
Zinc oxide  
Zn-Cu alloy

## ABSTRACT

To prepare well-defined models of ZnO-based catalysts, in particular of Cu/ZnO used for methanol synthesis, we studied the structure of Zn and ZnO thin films grown on a Cu(111) single crystal surface using metal vapor deposition. Structural characterization was performed by scanning tunneling microscopy, Auger electron spectroscopy, and low-energy electron diffraction. In agreement with previous studies, Zn wets the Cu surface forming mixed surface layer depending on Zn coverage. Surface oxidation of the Zn film into ZnO, as monitored by STM, showed that the reaction starts at step edges and propagates inside the terrace at increasing temperature. However, the process is affected by Zn migration into the Cu bulk and hence the film formation critically depends on the heating rate. In another approach using Zn deposition in oxygen ambient and subsequent annealing in vacuum, the resulted films were well-ordered and showed a long-range coincidence structure, assigned to the formation of a single ZnO(0001) layer on top of Cu(111). Independent of preparations conditions, the ZnO overlayer did not cover the entire surface, leaving considerable areas exposing Cu(111) or Cu<sub>2</sub>O/Cu(111) surface. Reactivity measurements for CO oxidation and reverse water gas shift reactions at nearly atmospheric pressures showed no promotional effects of the ZnO overlayer under conditions studied. Moreover, Zn irreversibly migrates into the Cu crystal bulk in an O<sub>2</sub> rich ambient, and the surface chemistry is governed, in essence, by a poorly defined Cu-oxide film. However, the ZnO/Cu model catalysts are fairly stable in a mixture of CO<sub>2</sub> and H<sub>2</sub>.

## 1. Introduction

Zinc oxide (ZnO) based catalysts show superior performance in methanol synthesis and water gas shift (WGS) reactions. Although Cu/ZnO/Al<sub>2</sub>O<sub>3</sub> catalysts are commercially used in industry, the atomic structure of active sites in these catalysts remains debated in the literature. Among many proposed structures and reaction mechanisms, the crucial role of the ZnO/Cu interface has been highlighted (Refs. [1,2] and references therein). However, the metallic Zn-Cu sites were also considered as active [3–5]. In addition, several models invoke structures formed by Cu nanoparticles encapsulated by very thin ZnO overlayer [6–8]. This situation motivates research groups to perform studies on planar model systems such as metallic Cu nanoparticles and clusters deposited on ZnO single crystal surfaces [9–11]. Also the atomic structure and the formation of the Cu–Zn surface alloy received much attention. [12–14] In this respect, ZnO thin films supported on Cu can be considered as well-suited model systems for studying the reaction at the interface in order to rationalize the critical role of a ZnO phase in these catalysts. Moreover, ultrathin films supported on metals may show interesting catalytic properties in their own right [15–19].

Studies focusing on preparation of ZnO films on Cu single crystals

and foils were initiated more than twenty years ago using oxidation of metallic Zn overlayers [11,13,20–22]. Several attempts were made to fabricate thin ZnO films by oxidation of brass. [23] However, well-ordered ZnO films were not obtained in these studies. Preparation of crystalline ZnO films was first reported for a Ag(111) substrate employing pulsed laser deposition and vacuum annealing [24]. To date, crystalline ZnO films growing in the (0001) orientation have been prepared on Pd(111) [25], Pt(111) [26,27], and Au(111) [28]. On the basis of theoretical calculations, it is generally accepted that ZnO as an ultrathin film relaxes into a “depolarized” structure, in which Zn and O atoms are arranged in almost coplanar sheets as in the hexagonal boron-nitride structure.

In this work, we address the preparation of ZnO films on Cu(111) as a well-defined model system which could shed more light on chemistry of ZnO based catalysts. For this we use two different approaches frequently used in thin film growth. In the first one, Zn was vapor deposited onto clean Cu(111) and subsequently oxidized under UHV compatible pressure conditions. In the second approach, we employed Zn deposition in an oxygen ambient (so called “reactive” deposition) followed by annealing in vacuum. The structural characterization of the model catalysts was performed by scanning tunneling microscopy

\* Corresponding author.

E-mail address: [shaikhutdinov@fhi-berlin.mpg.de](mailto:shaikhutdinov@fhi-berlin.mpg.de) (S. Shaikhutdinov).

(STM), Auger electron spectroscopy (AES), and low energy electron diffraction (LEED). We also report results on the reactivity of this model system for CO oxidation and reverse (r-) WGS reactions at nearly atmospheric pressures and on structural and compositional changes induced by reaction ambient.

## 2. Experimental

The experiments were performed in an ultrahigh vacuum (UHV) chamber equipped with an STM (Omicron) and a four grid optics LEED apparatus used also for AES (from Specs). The Cu(111) crystal was clamped to an Omicron sample holder. The sample temperature was measured by a Type K thermocouple put into a small hole at the edge of the crystal. Clean surfaces were obtained by cycles of Ar<sup>+</sup>-sputtering and annealing in UHV and 10<sup>-7</sup> mbar O<sub>2</sub> to remove residual carbon. Zinc was deposited by heating a Zn rod (1 mm in diameter, 99.99%, Goodfellow) to 500 – 525 K by passing current through a thoriated tungsten wire wrapped around the rod. The deposition flux was controlled via the Zn rod temperature measured by a Type K thermocouple spot-welded to the edge of the rod. The Zn source is shielded by a metal cylinder having a small orifice (~ 5 mm in diameter) and placed about 2 cm away from a crystal.

STM images were obtained with commercial Pt-Ir tips (L.O.T.-Oriel) using tunneling parameters in the range of 1 – 2 V (bias) and 0.5–1 nA (current). The images were only subjected to plane corrections, if not specified.

## 3. Results and discussion

In the first approach, we employed Zn physical vapor deposition in UHV at room temperature and subsequent oxidation in 10<sup>-6</sup> mbar pressure range at elevated temperatures. The amount of Zn deposited onto the clean Cu(111) was monitored by AES using the ratio of Zn (at 994 eV) and Cu (at 776 eV) peaks. Albeit the latter signal is significantly lower in intensity as compared to the principal Auger signal for Cu at 920 eV, it is the only one that does not overlap with the Auger transitions of Zn. Henceforth, this Auger ratio was used as a measure of the Zn coverage. Large-scale STM images (Fig. 1) of Zn/Cu(111) films at various amounts of deposited Zn showed no three-dimensional particles and aggregates, but flat terraces and ad-islands. This suggests that metallic Zn grows on Cu(111) in a layer-by-layer mode, as previously proposed on the basis of TPD and XPS results [14]. For the formation of a fully covered Zn monolayer, an estimate based on AES analysis [29] results in the above-mentioned Auger ratio value of ~ 1 (using a Zn layer thickness = 2 Å, and the mean free path of electrons = 10 Å). The STM images at such ratios (Fig. 1a) revealed wide terraces and

irregularly shaped patches with a broad size distribution, probably due to a coalescence of smaller islands. When these islands merge with the step edges they do not exhibit any boundary with respect to a high-lying terrace, indicating that they share the same surface structure. Indeed, the monoatomic steps on Cu(111) (= 2.08 Å) and Zn(0001) (= 2.47 Å) differs substantially and hence must be readily detectable by STM. A peninsular-like morphology of the step edges clearly differs from that observed on the clean Cu(111) surface (inset in Fig. 1b). Such morphology can be rationalized in terms of Zn-Cu surface alloying, albeit the latter is thought to occur at higher temperatures [12,14]. Although the basal Zn(0001) surface has a much lower surface energy as compared to Cu(111) (i.e., 0.99 and 1.95 J/m<sup>2</sup>, calculated [30]), previous STM studies [12] of the initial stages of Zn deposition on Cu(111) provided solid evidence that Zn ad-atoms substitute Cu in the surface layer at 300 K, in agreement with DFT calculations [31].

It has previously been proposed that Zn atoms adsorb at step edges and then migrate inside the upper terrace layer until a homogeneous distribution in the surface layer is reached. This scenario was inspected by theoretical calculations using Monte-Carlo simulations [32]. The results suggested that, at low coverage (0.25 ML), Zn ad-atoms coalesce forming compact islands with edges along the close-packed direction. At and above room temperature, the place exchange between the Zn ad-atoms and Cu atoms in upper terrace sets in, which is accompanied by the formation of Zn-decorated Cu islands. As the Zn coverage increases, an intermixing is less pronounced, favoring the formation of larger Zn islands within the adlayer, stable at higher temperatures. For 0.9 and 1.5 ML Zn, similar features are observed by simulations, i.e. the formation of a mixed, largely disordered Cu-Zn upper layer. Since the proposed Zn-Cu surface alloying mechanism involves surface diffusion, the resulted surfaces in our films may additionally be affected by the deposition flux.

Although it is difficult to discriminate pure Cu(111) and mixed Zn-Cu(111) surfaces in the presented STM images lacking atomic resolution, their close inspection showed that the step heights between the adjacent terraces (or patches) are often not identical. For example, the height difference between the areas labelled A and B in Fig. 2 is about 0.2 Å higher than between C and B. (The absolute step heights measured by STM (all in 2–2.5 Å range) may deviate depending on the tip and tunneling conditions). In addition, the areas B and C (but not A) show a long range modulation seen in STM as an irregular network of depressed lines (inset in Fig. 2b). In principle, this finding may be explained by Zn-Cu surface alloying, taking into account the difference in density of atoms in a mixed Zn-Cu layer (depending on Zn/Cu ratio) and the Cu(111) surface underneath, which may result in structure to some extent similar to the well-known “herring bone” reconstruction on the Au(111) surface. Another possible explanation would have to take

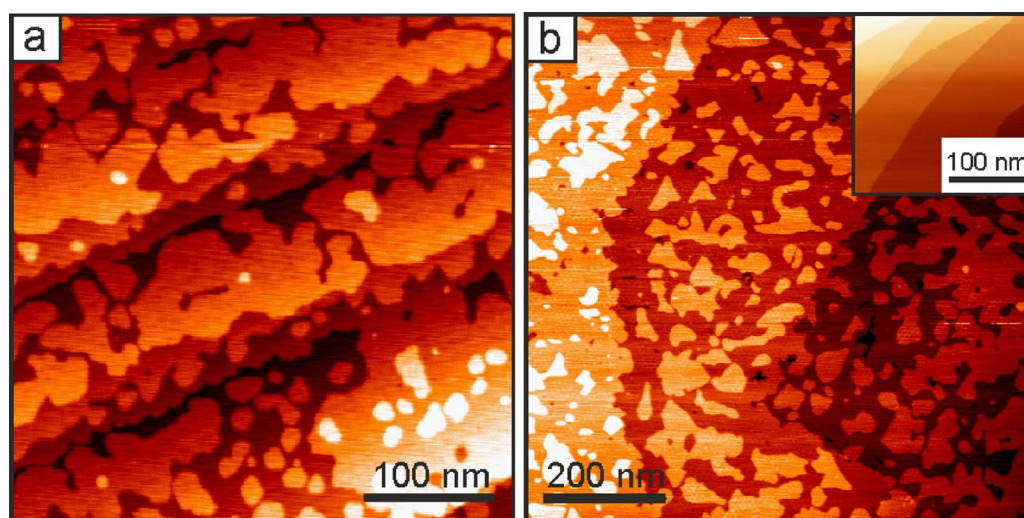


Fig. 1. STM images of Zn films on Cu(111) at 1.2 (a) and 2.5 ML (b) coverages determined by AES. Inset displays the STM image of the clean Cu(111) surface for comparison.

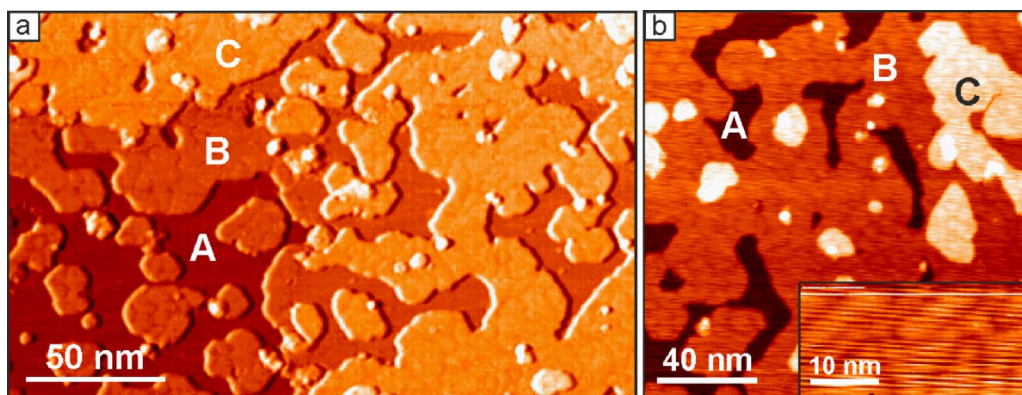


Fig. 2. STM images of the 1 ML Zn/Cu(111) surface. Image (a) is presented in differentiated contrast. The regions labelled B and C exhibit domain structure (shown in inset), whereas the regions A does not. The step height measured between regions B and A is about 0.2 Å larger than between C and B.

into account the difference in surface lattice constants of Cu(111) and Zn (0001). Since at all Zn coverages studied here, LEED patterns showed only  $(1 \times 1)$  diffraction spots of Cu(111), the pure Zn ad-layer, if formed, must follow the Cu(111) lattice. However, because of the  $\sim 4\%$  mismatch between the Zn(0001) and Cu(111) lattices (2.67 and 2.55 Å, respectively), a single Zn layer on top of Cu(111) would experience a certain strain which may be relieved via domain structure as observed by STM. In any case, such regions must be attributed to Zn-containing surfaces. As the A/B step height is not equal to that of the B/C step, the area C must be assigned to a second Zn-Cu layer rather than to a first layer on top of a Cu(111) large island underneath.

At increasing Zn coverage (Zn/Cu Auger ratio  $> 2.5$ ), STM images revealed a long-range periodic structure (Fig. 3a), which, to the best of our knowledge, has never been reported for Zn/Cu(111) surfaces. In fact, two different structures are observed. The one (labelled M in Fig. 3b) shows a wave-like morphology typical for the Moire-type coincidence structures. The other one exhibits a honeycomb-like morphology (labelled H). The periodicity measured by STM for the M and H structures are about 4.8 and 8 nm, respectively, and structure H is rotated by  $30^\circ$  with respect to structure M. Unfortunately, atomic resolution could not be achieved to identify the structures in more detail, and also LEED inspection showed no additional diffraction spots which would allow to measure the lattice constants more precisely. Interesting also is that the topmost islands primarily exhibit a triangular shape.

In principle, the formation of superstructures is a typical phenomenon for thin film growth, when an overlayer exhibits a small lattice mismatch to a substrate. In the case of a Zn(0001) layer, having the same surface lattice as in the bulk ( $= 2.67$  Å), that is placed on top of Cu(111) ( $= 2.55$  Å) along the main crystallographic direction, one can find a coincidence structure with a periodicity 56 Å (i.e. 21 lattices of Zn(0001) coinciding with 22 lattices of Cu(111), since

$21 \times 2.67 \cong 22 \times 2.55$  Å). This value falls in the range obtained for structure M ( $\sim 48$  Å). Accordingly, the H structure shows a  $(2 \times 2)$   $R30^\circ$  structure with respect to the M structure, thus resulting in a  $48 \times \sqrt{3} = 83$  Å periodicity, which is also close to the experimentally observed value of 80 Å.

Therefore, the above-presented results show that Zn readily wets the Cu(111) surface, and the morphology, surface composition and long-range ordering depends on Zn coverage and other parameters affecting Zn-Cu intermixing in the surface layer(s). In principle, this conclusion is in good agreement with a very recent XPS and DFT study [33] suggesting the formation of a two atomic-layer Zn-Cu alloy by Zn deposition on Cu(111) at 300 K. Note, however, that the formation of three-dimensional Zn islands on top of the alloyed surface at coverages above 1 ML, as proposed on the basis of quantitative analysis of their XPS and UPS results, is not observed here.

In the next step, we studied oxidation of a Zn/Cu(111) surface in order to form crystalline ZnO films. To monitor the oxidation process, we examined the 1 ML Zn/Cu(111) sample by LEED, AES and STM after exposures to  $10^{-6}$  mbar of  $O_2$  for 5 min at temperatures increased stepwise between 300 and 550 K. Fig. 4 displays large-scale STM images at temperatures as indicated, with corresponding LEED patterns shown in insets. Auger spectra and their analysis are presented in Fig. S1 in the Supplementary Materials (SM).

Oxygen exposure causes surface oxidation even at room temperature as observed by AES (Fig. S1a). The corresponding STM image clearly shows that all step edges are decorated, whereas the internal areas within the terraces remain flat and keep showing domain structure observed prior to the oxygen exposure (see Fig. 2b). The apparent height of newly formed species at step edges is about 3.5 Å with respect to the low-lying terrace, or about 1 Å to the upper terrace. The reaction further develops upon oxidation treatments at 350 and 400 K.

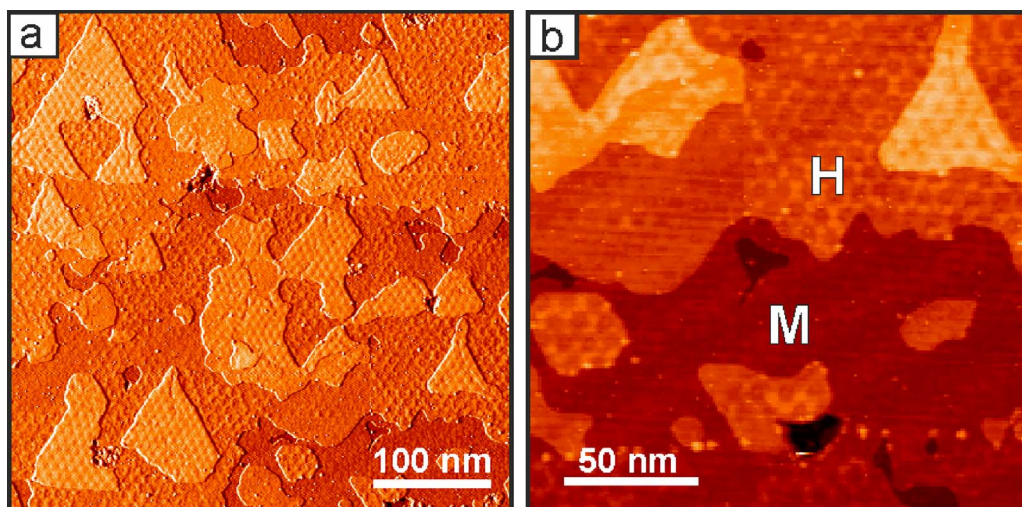


Fig. 3. STM images of 2.5 ML Zn/Cu(111) films showing Moire-like (labelled M) and honeycomb-like (H) structures.

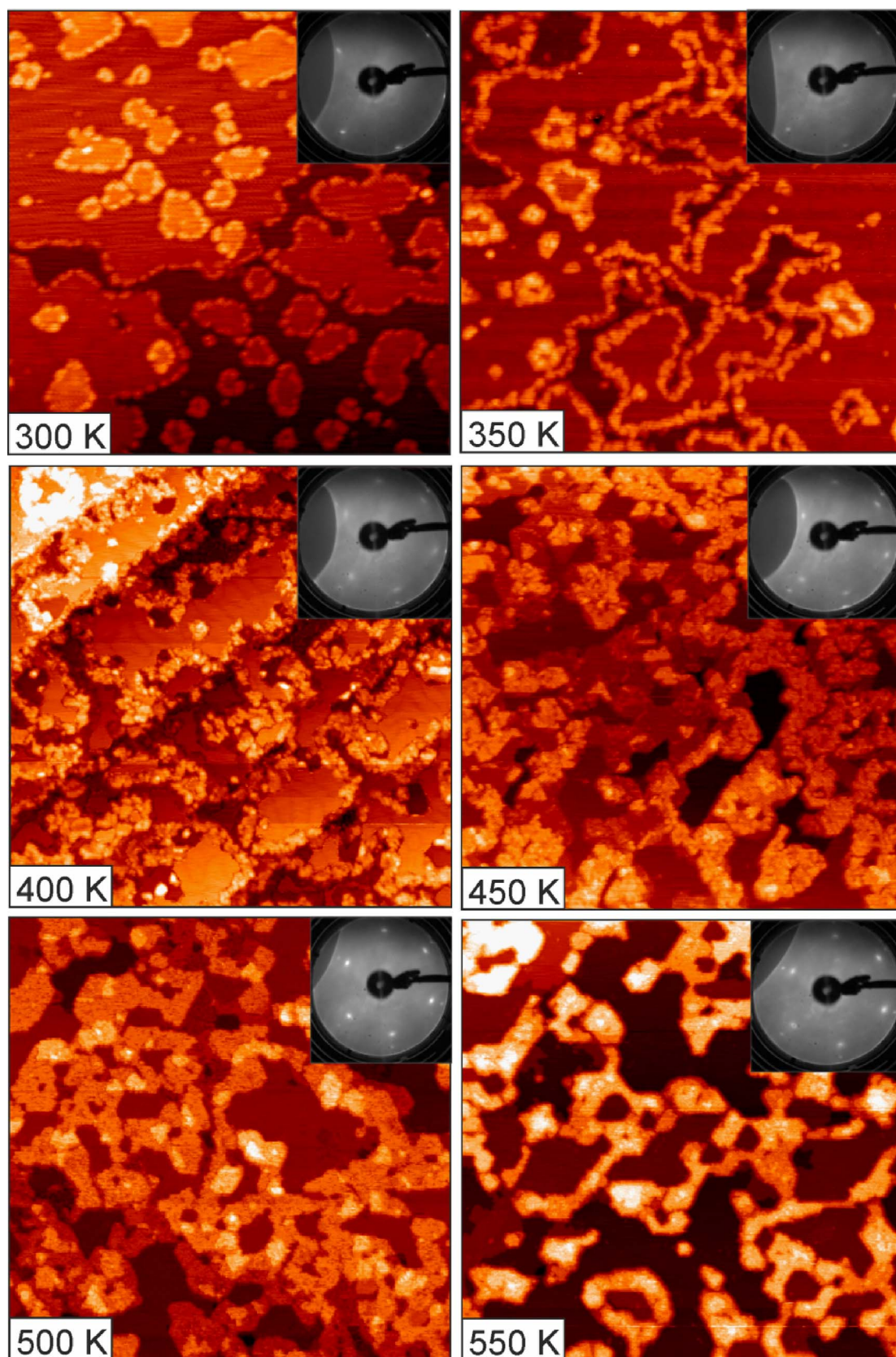


Fig. 4. Large-scale (all  $200 \text{ nm} \times 200 \text{ nm}$ ) STM images of 1 ML Zn/Cu(111) after subsequent oxidation in  $10^{-6}$  mbar  $\text{O}_2$  at temperature increased stepwise (as indicated). The corresponding LEED patterns are shown in insets.

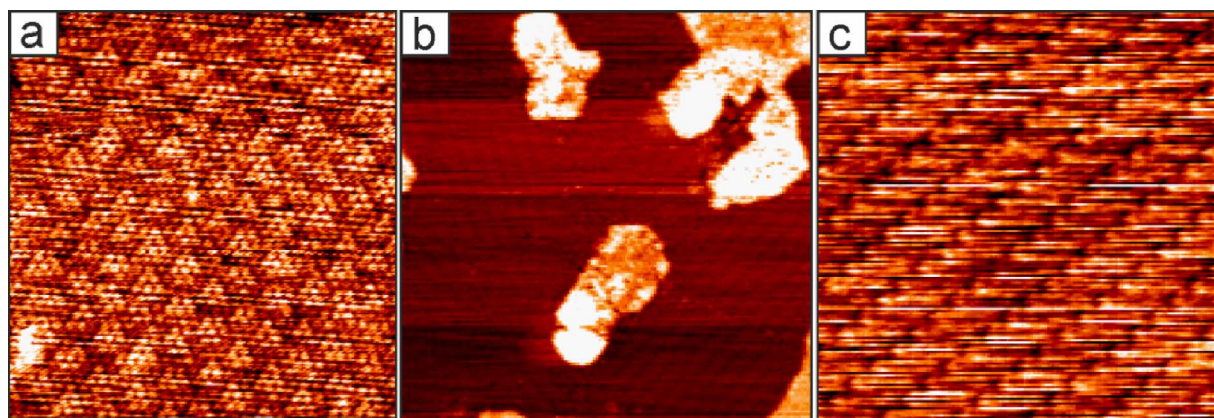


Fig. 5. (a) High-resolution STM image of the region between ZnO islands formed by oxidation at 550 K (see Fig. 4). The protrusions with a 6 Å periodicity shows superstructure which is similar to the one previously reported for the ‘44’-Cu<sub>2</sub>O/Cu(111) surface [35]. (b) Rotational domains with a stripe-like structure seen between the ZnO islands are virtually identical to that obtained for clean Cu(111) after oxidation at 600 K, as shown in image (c), and previously assigned to ‘29’-Cu<sub>2</sub>O/Cu(111) [35].

Accordingly, the amount of oxygen in the sample gradually increases and saturates at 450 K (Fig. S1b), whereas the LEED patterns show additional diffraction spots (whose intensity maximizes at 500 K), which are aligned with those of Cu(111) and correspond to ZnO(0001) [25,27]. The height of irregularly shaped ZnO islands and particles at step edges increases up to 6 Å by oxidation at 450 K, and the original domain structure is no longer observed on flat terraces between the islands. Instead, these regions exhibit long-range periodic structures (Fig. 5a,b). Such superstructures were observed on Zn-free Cu(111) surfaces after similar oxidation treatments and look virtually identical to those reported for so-called ‘44’ and ‘29’ structures of Cu<sub>2</sub>O layer, which were named according to their unit cells, which are 44 and 29 times larger than the one of Cu(111) [34–37]. The formation of a Cu<sub>2</sub>O layer in our samples was also identified by LEED (see Fig. S2 in SM) showing a pattern similar to those previously reported. Ultimately, at 550 K, the ZnO islands grow in height (up to 9 Å) with a concomitant decrease of surface coverage, thus suggesting film dewetting.

The results presented above show that oxidation of Zn deposits on Cu(111) leads to the formation of (0001)-oriented ZnO islands. It appears that the oxidation temperature around 550 K is optimal for the preparation of well-ordered ZnO(0001) films. It turned out, however, that oxidation of the Zn/Cu(111) surface by heating directly to 500 K (i.e. not in a stepwise manner as used above) led to substantial (often almost complete) loss of Zn at the surface (measured by AES), even by initial deposition of large amounts of Zn. For example, Fig. 6a displays a 3 ML Zn film oxidized at 500 K, showing solely small ZnO islands decorating step edges, whereas the terraces expose a Cu<sub>2</sub>O/Cu(111) surface. In contrast, all samples oxidized stepwise showed no loss of Zn as judged by AES. It has previously been reported that Zn deposits on Cu(111) desorb in the temperature range between 500 and 640 K [13,14]. Once formed, ZnO species desorbs at temperatures as high as 850 K [13]. Fig. 6b shows STM image of the film prepared by stepwise oxidation of 1.7 ML Zn overlayer to 500 K in 10<sup>-6</sup> mbar O<sub>2</sub> which almost fully covers a Cu(111) substrate. Annealing in UHV at 550 K for 10 min does not result in considerable changes (Fig. 6c), thus suggesting that the film is thermally stable. It appears, however, that annealing at higher temperatures causes film dewetting (Fig. 6d,e). Exposure to 5 mbar of H<sub>2</sub> at 500 K does not show considerable effects on the film morphology either (Fig. 6f).

Therefore, in our experiments using heating to 500 K in oxygen ambient, Zn migrates into the Cu bulk rather than desorbs into the vacuum. Accordingly, the film growth kinetics involves not only the oxidation process itself, but also Zn migration into the deeper Cu layers, both processes being thermally activated. Therefore, the resulting structure may depend on the heating rate as well. On the basis of STM images shown in Fig. 4, it is clear that oxidation starts at step edges, where O<sub>2</sub> dissociation on low-coordination sites is apparently more

facile, and where, in addition, Zn concentration appears to be higher [12]. The reaction propagates further at increasing temperature which is accompanied by depletion of Zn in the topmost Zn-Cu layer, ultimately resulting in a Zn-free Cu(111) surface which may also undergo oxidation, thus leading to a complex Cu<sub>2</sub>O/Cu(111) surface. In the case of fast heating, however, Zn atoms in the interior parts of the mixed Zn-Cu terraces diffuse into the sub-surface region and become unavailable for oxidation. As a result, only small ZnO islands at step edges are formed (Fig. 6a), whereas the great majority of Zn migrated into Cu.

In order to prevent Zn intermixing with Cu during deposition step and subsequent migration during oxidation treatment, in the next approach we employed Zn deposition in oxygen ambient (“reactive deposition”). Since in our setup Zn deposition could only be performed at 300 K, and bearing in mind the relatively low sticking coefficient for O<sub>2</sub> on Cu(111), (ref. [38] and references therein) we deposited Zn in 10<sup>-5</sup> mbar of O<sub>2</sub>.

Fig. 7a shows an STM image of the film prepared using Zn deposition parameters (flux and exposure) leading to the deposition of about 1 ML of Zn (NB: the sticking coefficient under these conditions remains unknown). The surface of this “as deposited” film is highly corrugated and showed, in essence, a disordered structure. The film becomes considerably smoother after UHV annealing at 450 K (Fig. 7c). Concomitantly, streaky diffraction spots of ZnO(0001) appear, indicating a coexistence of slightly misaligned ZnO domains. A long-range ordering is clearly seen in STM images via a Moire-like structure with a ~ 13.5 Å periodicity (Fig. 8a). The latter can readily be explained by a coincidence structure, where four unit cells of ZnO(0001) coincide with five unit cells of Cu(111) (i.e. 4 × 3.25 Å ≈ 5 × 2.55 Å). This superstructure further develops upon annealing at 500 and 550 K (Fig. 8b,c) and is also reflected in corresponding LEED patterns (Fig. 7). At higher temperatures (600 K), the film dewets, thus resulting in large, irregularly shaped ZnO islands and a clean Cu(111) surface. Therefore, as in the case of ZnO films produced by oxidation of metallic Zn layers, the annealing temperatures to prepare well-ordered films fall in the range of 500–550 K.

The terraces are not uniformly covered. In addition to the areas showing a Moire structure and dominating the film surface, many small regions, imaged as depressed islands, showed no atomic corrugation and were, therefore, assigned to a bare Cu(111) substrate. In turn, these islands exhibit different height and labelled Cu1 and Cu2 in Fig. 8, respectively. The height difference between those (about 2.1 Å, see profile lines in Fig. 8) matches the interlayer distance in Cu(111) (= 2.08 Å). The height difference between the Moire areas, labelled M1 and M2, is 2.1 Å, and hence can be assigned to the same ZnO layer following the morphology of the Cu support underneath. In turn, the M2-Cu2 and M1-Cu1 distances are both about 1.8 Å, indicating that the ZnO film is only one layer in thickness, which is also consistent with the

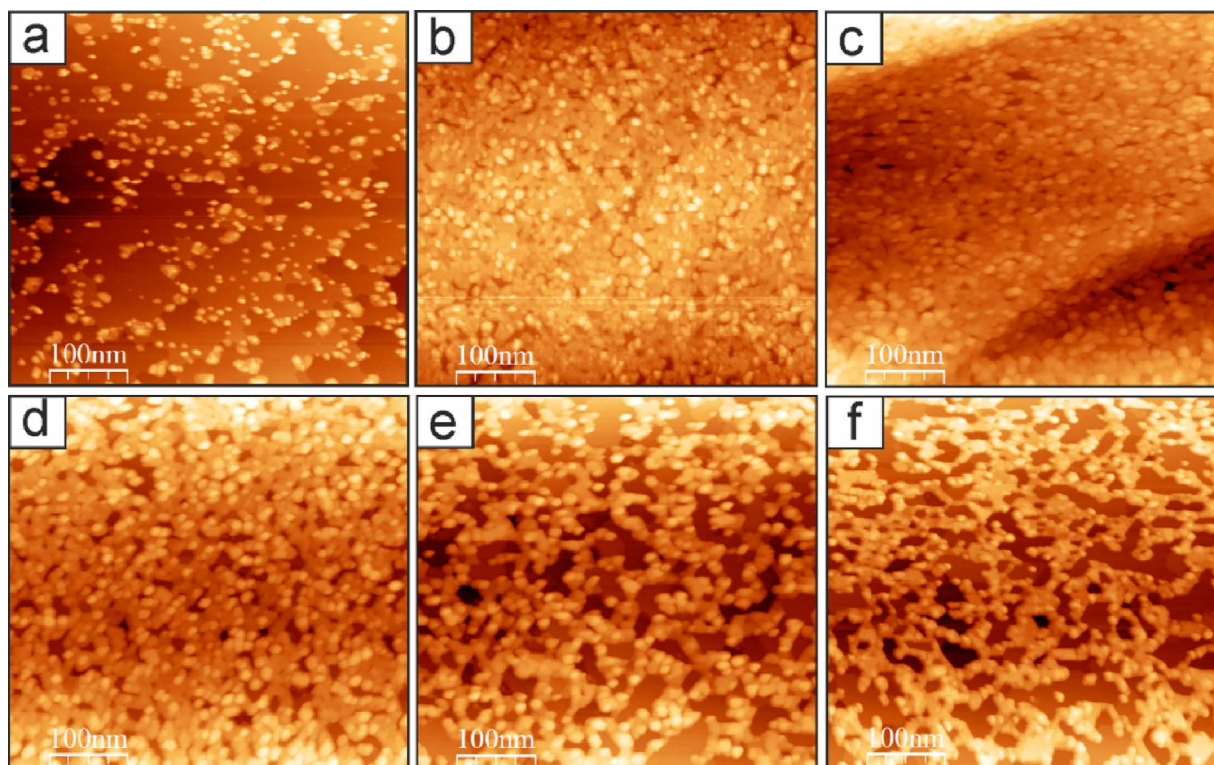


Fig. 6. Large-scale (500 nm  $\times$  500 nm) STM images of: (a) 3 ML Zn/Cu(111) surface after “fast heating” oxidation in  $10^{-6}$  mbar  $O_2$  at 500 K; (b) 1.7 ML Zn/Cu(111) surface after “stepwise oxidation” to 500 K. Then the sample was annealed in UHV at 550 (c), 600 (d), and 650 K (e), respectively, for 10 min at each temperature. Image (f) obtained after subsequent exposure to 5 mbar  $H_2$  at 500 K for 10 min.

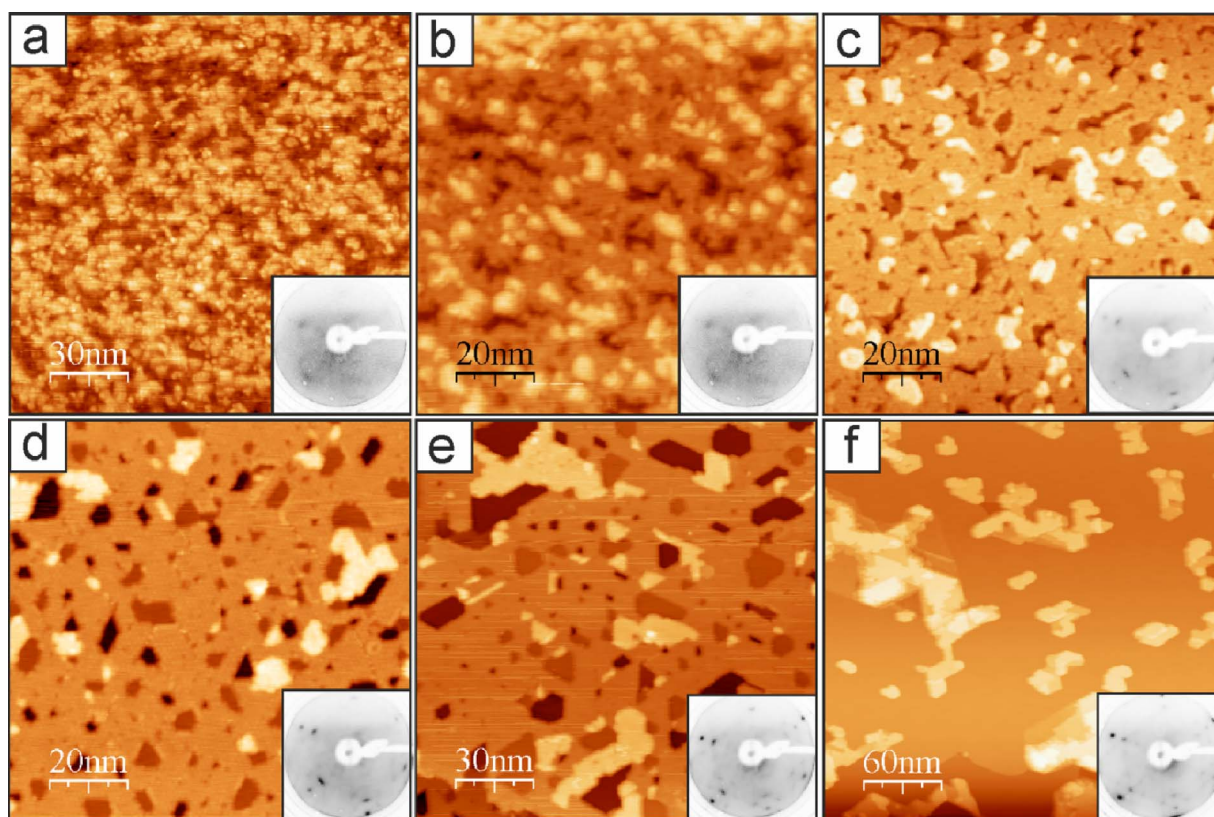
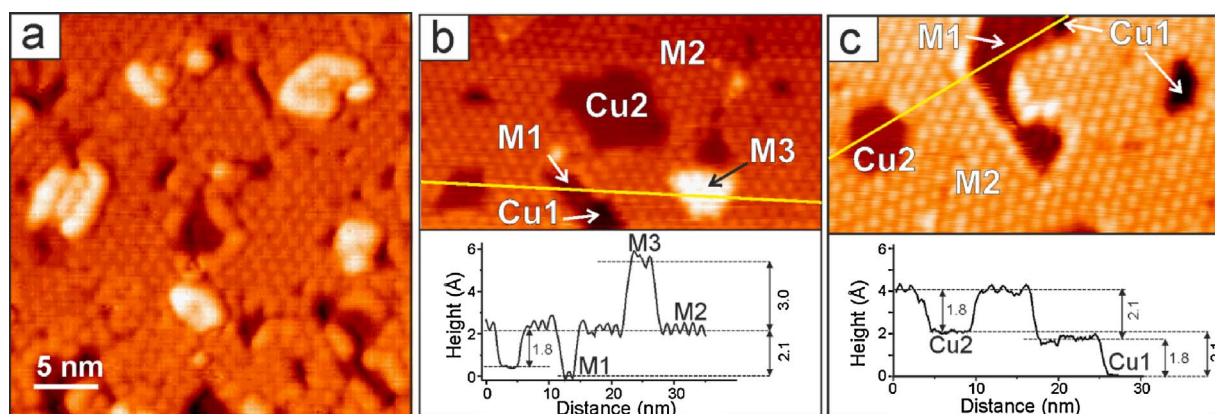


Fig. 7. STM images and LEED patterns (as insets, inverse contrast) of a ZnO film prepared by 1 ML Zn deposition in  $10^{-5}$  mbar  $O_2$  at 300 K (a) followed by UHV annealing at 400 (b), 450 (c), 500 (d), 550 (e), and 600 K (f), respectively, for 10 min at each temperature.



**Fig. 8.** Close-up STM images of the film (large-scale images are shown in Fig. 7) annealed at 450 (a), 500 (b), and 550 K (c). Image (a) is presented in differentiated contrast. The profile lines are shown below the images (see text).

amount of Zn ( $\sim 1$  ML) measured by AES. In addition, small ad-islands (labelled M3), also showing the Moire pattern, are observed. In contrast, these islands are about  $3 \text{ \AA}$  in height with respect to M2 (i.e. considerably higher than the above-discussed values of 1.8 and  $2.1 \text{ \AA}$ ) and therefore may be assigned to a second layer of ZnO.

STM measurements of numerous films prepared at various amounts of deposited Zn revealed very similar morphology, where a ZnO(0001) layer coexisted with areas exposing a bare Cu(111) substrate visible as depressed islands and pits. It seems plausible that even under reactive deposition conditions at room temperature Zn intermixes with O and Cu at the surface and form a non-stoichiometric Zn-Cu-O mixed layer which “disproportionates” into ZnO(0001) and Cu(111) surface phases upon annealing in UHV, thus making it difficult to prepare a fully closed film. Solely increasing Zn deposition time could not change the picture. Increasing Zn exposure from 20 min (used above) to 3 h only slightly increased ZnO coverage in both, “as deposited” films and UHV annealed films (see Fig. S3 in SM). Interestingly, such a “self-limited” film growth was also observed while preparing ZnO film on Ag(111). Its origin remains unclear and needs further investigations.

Finally, we examined the reactivity of ZnO/Cu(111) films for CO oxidation and r-WGS reactions. The experiments were performed in another UHV chamber, equipped with LEED and AES, which additionally houses a gold-plated reaction cell ( $\sim 30$  ml) connected to a gas chromatograph (Agilent). A double-side polished Cu(111) crystal was spot-welded to Ta wires for resistive heating. The crystal could be transferred into the reaction cell and sealed via a Viton ring. For CO oxidation, the reaction mixture consisted of 10 mbar CO and 50 mbar

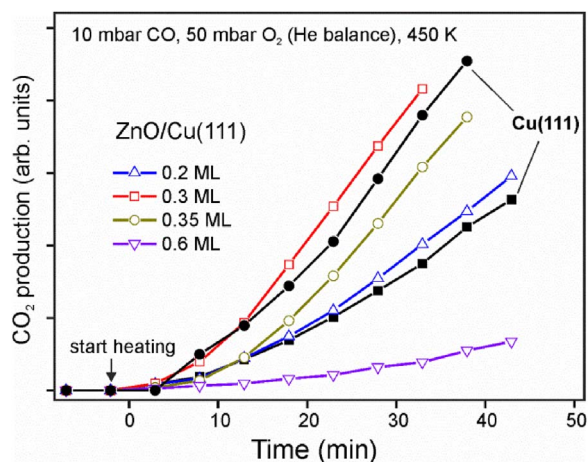


**Fig. 9.** Kinetics of  $\text{CO}_2$  production measured in mixture consisting of 10 mbar of CO and 50 mbar of  $\text{O}_2$  (He balanced to 1 bar) on ZnO/Cu(111) at coverages as indicated. The results for two pure Cu(111) samples are shown for comparison.

$\text{O}_2$  (balanced by He to 1 bar). For the r-WGS reactions, the mixture of 50 mbar  $\text{CO}_2$  and 50 mbar  $\text{H}_2$  (He balanced) was used. The gases were dosed at room temperature and slowly circulated, using a membrane pump, for about 20 min to stabilize GC signals. Then the sample was heated to the reaction temperature (450 K in both cases) with a rate of  $1 \text{ K s}^{-1}$ .

Fig. 9 shows the  $\text{CO}_2$  production measured on ZnO/Cu films at various coverages as a function of time. For comparison, results of the blank experiments on two bare Cu(111) samples are also presented,

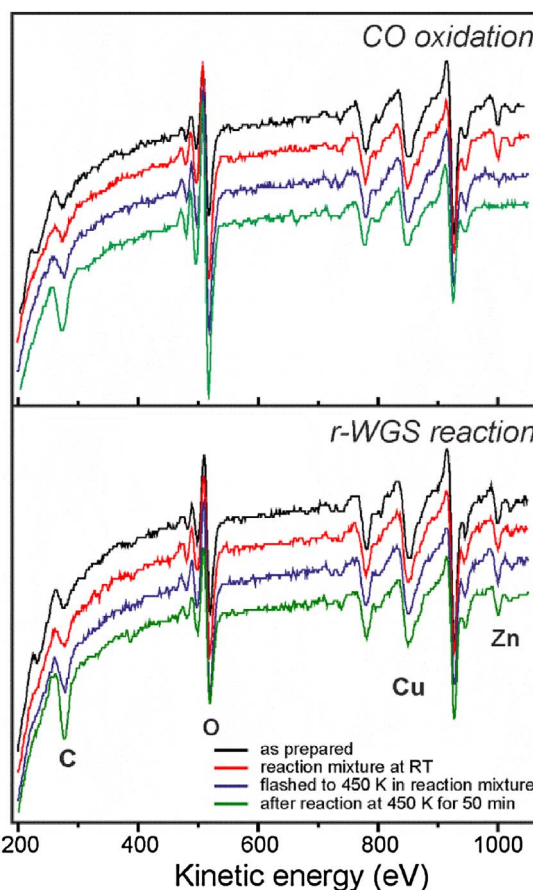


**Fig. 10.** Auger spectra recorded on  $\sim 0.6$  ML ZnO/Cu(111) films as prepared (black lines) and sequential exposure to the reaction mixtures (10 mbar CO + 50 mbar  $\text{O}_2$ ; 50 mbar  $\text{CO}_2$  + 50 mbar  $\text{H}_2$ , (all He balanced) for the CO oxidation and r-WGS reactions, respectively, at 300 K (red), after thermal flash to 450 K in reaction mixture (blue) and after 50 min at 450 K (green). (For interpretation of the references to colour in this figure legend, the reader is referred to the web version of this article.)

which revealed that activity considerably scatters even on the virtually identical clean Cu surfaces. Apparently, at low coverages ZnO does not show any significant effect, as the reaction rate falls into the range observed for bare Cu(111). However, increasing the coverage to  $\sim 0.6$  ML definitely suppresses activity. In essence, no promotional effect of ZnO is observed for CO oxidation on Cu, at least under our reaction conditions.

Interestingly, post-characterization of the spent catalysts by AES revealed no Zn in the surface layers. Additional AES measurements on ZnO/Cu films after sequential treatments (Fig. 10, top panel), showed that exposure to the reaction mixture at 300 K considerably increases the O signal. Concomitantly, the Cu(111)-related diffraction spots disappear while the ZnO(0001) spots become diffuse, all suggesting the formation of a disordered  $\text{CuO}_x$  overlayer between the ZnO islands. However, thermal flash of the sample to 450 K in the reaction mixture results in strong attenuation of the Zn signal in Auger spectra and of the ZnO(0001) diffraction spots in LEED, but in considerable (by factor of 2) increase of the O amount. Ultimately, the ZnO fingerprints totally vanish at longer exposures. Since ZnO sublimes at much higher temperatures [27], the results suggest Zn migration into the Cu crystal bulk. As subsequent annealing in oxygen could not recover the ZnO phase, Zn seems to migrate quite deep inside. Therefore, under CO oxidation reaction conditions, the reaction is, in fact, governed by a thin disordered  $\text{CuO}_x$  film, which may, however, be affected by the ZnO overlayer initially present in the catalyst.

For the r-WGS reaction, the measurements performed on 0.6 ML ZnO/Cu(111) films did not show any activity in terms of CO formation under the conditions studied. We monitored structural and compositional changes by AES and LEED in the same manner as described above. Fig. 10 (bottom panel) depicts AES spectra of the “as prepared” film and after sequential exposure of the film to reaction gases at 300 and 450 K. In contrast to  $\text{CO} + \text{O}_2$ , in  $\text{CO}_2 + \text{H}_2$  atmosphere all Auger signals remains unchanged, except of carbon, which continuously increases for longer reaction times (both in CO and r-WGS reactions, though). In the r-WGS reaction ambient, the ZnO diffraction pattern attenuates, but does not disappear even after 50 min at 450 K, thus indicating that the ZnO(0001) islands remain fairly stable. This is also supported by the STM image presented in Fig. 6f, showing that the morphology of the ZnO phase remains basically the same after exposure to 5 mbar of  $\text{H}_2$  at 500 K.

Therefore, the comparison of ZnO/Cu(111) catalysts in two different reactions clearly show that structural and compositional changes may occur at surface under near atmospheric pressure conditions which are strongly dependent of the reaction conditions.

#### 4. Conclusions

In this work, we studied the structure of ultrathin Zn and ZnO films formed on a Cu(111) single crystal surface using metal vapor deposition. Structural characterization performed by STM, LEED, AES showed that Zn readily wets the Cu surface forming mixed surface layer depending on Zn coverage. Oxidation of Zn layer into ZnO starts at step edges and propagates inside the terrace at increasing temperature. However, the process is influenced by Zn migration into the Cu bulk. Therefore, the resulting film structure critically depends on the heating rate. Zinc vapor deposition in oxygen ambient appears to suppress intermixing. Subsequent annealing in vacuum resulted in well-ordered ZnO films showing a long-range coincidence structure, assigned to the formation of a single ZnO(0001) layer on top of Cu(111). Independent of preparations conditions, the ZnO overlayer did not cover the entire surface, leaving considerable areas exposing the Cu substrate surface.

Reactivity measurements at partial pressures in the range of 10–50 mbar (He balanced to 1 bar) showed no promotional effects of ZnO overlayer on either CO oxidation or reverse WGS reactions, at least in our conditions. Moreover, ZnO irreversibly migrates into the Cu crystal bulk in CO oxidation at 450 K, such that the reactivity is, in

essence, governed by the  $\text{CuO}_x$  film. It appears that the prepared model catalysts are fairly stable under r-WGS reaction conditions. More elaborative reactivity studies remain to be done to elucidate structure-reactivity relationships using these model catalysts.

#### Acknowledgements

The work has been supported by Fonds der Chemischen Industrie, Deutsche Forschungsgemeinschaft through the Cluster of Excellence “UniCat”. BHL acknowledges the International Max Plank Research School “Complex surfaces in materials science”, and IMNG. thanks the Alexander von Humboldt Foundation for a fellowship.

#### Appendix A. Supplementary data

Supplementary data associated with this article can be found, in the online version, at <http://dx.doi.org/10.1016/j.apcata.2017.06.043>.

#### References

- [1] M. Behrens, F. Studt, I. Kasatkin, S. Kühl, M. Hävecker, F. Abild-Pedersen, S. Zander, F. Girgsdies, P. Kurr, B.-L. Knief, M. Tovar, R.W. Fischer, J.K. Nørskov, R. Schlögl, *Science* 336 (2012) 893–897.
- [2] S. Kattel, P.J. Ramírez, J.G. Chen, J.A. Rodriguez, P. Liu, *Science* 355 (2017) 1296–1299.
- [3] J. Nakamura, I. Nakamura, T. Uchijima, Y. Kanai, T. Watanabe, M. Saito, T. Fujitani, *J. Catal.* 160 (1996) 65–75.
- [4] S. Kuld, M. Thorhauge, H. Falsig, C.F. Elkjær, S. Helveg, I. Chorkendorff, J. Sehested, *Science* 352 (2016) 969–974.
- [5] J. Nakamura, Y. Choi, T. Fujitani, *Top. Catal.* 22 (2003) 277–285.
- [6] J.D. Grunwaldt, A.M. Molenbroek, N.Y. Topsøe, H. Topsøe, B.S. Clausen, *J. Catal.* 194 (2000) 452–460.
- [7] Y. Kanai, T. Watanabe, T. Fujitani, M. Saito, J. Nakamura, T. Uchijima, *Catal. Lett.* 27 (1994) 67–78.
- [8] R. Naumann d’Alnoncourt, X. Xia, J. Strunk, E. Löffler, O. Hinrichsen, M. Muhler, *Phys. Chem. Chem. Phys.* 8 (2006) 1525–1538.
- [9] M. Kroll, U. Köhler, *Surf. Sci.* 601 (2007) 2182–2188.
- [10] L.V. Koplitz, O. Dulub, U. Diebold, *J. Phys. Chem. B* 107 (2003) 10583–10590.
- [11] C.T. Campbell, K.A. Daube, J.M. White, *Surf. Sci.* 182 (1987) 458–476.
- [12] M. Sano, T. Adaniya, T. Fujitani, J. Nakamura, *J. Phys. Chem. B* 106 (2002) 7627–7633.
- [13] E.V. Thomsen, M. Christiansen, J. Onsgaard, *Appl. Surf. Sci.* 62 (1992) 189–194.
- [14] C. Ammon, G. Held, J. Pantförder, H.P. Steinrück, *Surf. Sci.* 482–485 (Part 2) (2001) 886–890.
- [15] H.-J. Freund, G. Pacchioni, *Chem. Soc. Rev.* 37 (2008) 2224–2242.
- [16] S. Shaikhutdinov, H.-J. Freund, *Annu. Rev. Phys. Chem.* 63 (2012) 619–633.
- [17] L. Giordano, G. Pacchioni, *Acc. Chem. Res.* 44 (2011) 1244–1252.
- [18] F.P. Netzer, F. Allegretti, S. Surnev, *J. Vac. Sci. Technol. B Microelectron. Nanometer Struct.* 28 (2010) 1–16.
- [19] E. Lundgren, A. Mikkelsen, J.N. Andersen, G. Kresse, M. Schmid, P. Varga, *J. Phys. Condens. Matter* 18 (2006) R481.
- [20] M. Sano, T. Adaniya, T. Fujitani, J. Nakamura, *Surf. Sci.* 514 (2002) 261–266.
- [21] J. Onsgaard, J.A. Bjo/rn, *J. Vac. Sci. Technol. A* 11 (1993) 2179–2185.
- [22] S.S. Fu, G.A. Somorjai, *Langmuir* 8 (1992) 518–524.
- [23] V. Schott, H. Oberhofer, A. Birkner, M. Xu, Y. Wang, M. Muhler, K. Reuter, C. Wöll, *Angew. Chem. Int. Ed.* 52 (2013) 11925–11929.
- [24] C. Tusche, H.L. Meyerheim, J. Kirschner, *Phys. Rev. Lett.* 99 (2007) 026102.
- [25] G. Weirum, G. Barcaro, A. Fortunelli, F. Weber, R. Schennach, S. Surnev, F.P. Netzer, *J. Phys. Chem. C* 114 (2010) 15432–15439.
- [26] B.-H. Liu, M.E. McBriarty, M.J. Bedzyk, S. Shaikhutdinov, H.-J. Freund, *J. Phys. Chem. C* 118 (2014) 28725–28729.
- [27] Y. Martynova, B.H. Liu, M.E. McBriarty, I.M.N. Groot, M.J. Bedzyk, S. Shaikhutdinov, H.J. Freund, *J. Catal.* 301 (2013) 227–232.
- [28] X. Deng, K. Yao, K. Sun, W.-X. Li, J. Lee, C. Matrangola, *J. Phys. Chem. C* 117 (2013) 11211–11218.
- [29] S. Ossicini, R. Memeo, F. Ciccacci, *J. Vac. Sci. Technol. A Vac. Surf. Films* 3 (1985) 387–391.
- [30] L. Vitos, A.V. Ruban, H.L. Skriver, J. Kollár, *Surf. Sci.* 411 (1998) 186–202.
- [31] Y. Morikawa, K. Iwata, J. Nakamura, T. Fujitani, K. Terakura, *Chem. Phys. Lett.* 304 (1999) 91–97.
- [32] S. Funk, G. Bozzolo, J.E. Garcés, U. Burghaus, *Surf. Sci.* 600 (2006) 195–204.
- [33] T. Koitaya, Y. Shiozawa, Y. Yoshikura, K. Mukai, S. Yoshimoto, S. Torii, F. Muttaqien, Y. Hamamoto, K. Inagaki, Y. Morikawa, J. Yoshinobu, *Surf. Sci.* 663 (2017) 1–10.
- [34] F. Jensen, F. Besenbacher, E. Lægsgaard, I. Stensgaard, *Surf. Sci. Lett.* 259 (1991) L774–L780.
- [35] T. Matsumoto, R.A. Bennett, P. Stone, T. Yamada, K. Domen, M. Bowker, *Surf. Sci.* 471 (2001) 225–245.
- [36] G. Gattinoni, A. Michaelides, *Surf. Sci. Rep.* 70 (2015) 424–447.
- [37] M. Sano, T. Adaniya, T. Fujitani, J. Nakamura, *Surf. Sci.* 514 (2002) 261–266.
- [38] F. Wiame, V. Maurice, P. Marcus, *Surf. Sci.* 601 (2007) 1193–1204.